



HAL
open science

An implicit well-posed Lagrangian scheme for non viscous compressible fluids in high dimension

Stéphane Del Pino, Bruno Després, Alexiane Plessier

► **To cite this version:**

Stéphane Del Pino, Bruno Després, Alexiane Plessier. An implicit well-posed Lagrangian scheme for non viscous compressible fluids in high dimension. 2024. cea-04492829

HAL Id: cea-04492829

<https://cea.hal.science/cea-04492829>

Preprint submitted on 6 Mar 2024

HAL is a multi-disciplinary open access archive for the deposit and dissemination of scientific research documents, whether they are published or not. The documents may come from teaching and research institutions in France or abroad, or from public or private research centers.

L'archive ouverte pluridisciplinaire **HAL**, est destinée au dépôt et à la diffusion de documents scientifiques de niveau recherche, publiés ou non, émanant des établissements d'enseignement et de recherche français ou étrangers, des laboratoires publics ou privés.

An implicit well-posed Lagrangian scheme for non viscous compressible fluids in high dimension

Stéphane Del Pino*, Bruno Després† and Alexiane Plessier‡

March 6, 2024

Abstract

We construct an implicit first-order Lagrangian scheme to approximate inviscid compressible gas dynamics in dimension $d \in \{1, 2, 3\}$. Our main theoretical result is that this finite volume scheme is unconditionally stable with regard to the time step, which means that solutions provided by the scheme ensure positivity of density and growth of physical entropy for all $\Delta t > 0$. We detail the issues related to the displacement of the mesh in dimension $d \in \{1, 2, 3\}$. Finally we illustrate the theoretical results with basic tests.

1 Introduction

Our viewpoint is that the rigorous development of implicit solvers for hyperbolic systems of conservation laws could be highly beneficial for applications when the CFL condition is stringent as in our last mock ICF (Inertial Confinement Fusion) calculation. In this direction, the notion of a Riemann solver which is by essence an explicit method [22, 25] is of little help. Instead, elaborating on our first work in 1D [20], we propose an implicit first-order Lagrangian scheme to approximate inviscid compressible gas dynamics in dimension $d \in \{1, 2, 3\}$. Our main theoretical result is that this finite volume scheme is unconditionally stable with regard to the time step, which means that for all time step $\Delta t > 0$ the solution of the nonlinear scheme always exists under natural physical conditions and that it satisfies positivity of density and growth of physical entropy. This is an extension to higher dimensions of our previous work [20] in dimension $d = 1$. Following the ideas of Chalons-Coquel-Marmignon [7], we use an isentropic predictor and a conservative corrector. We treat the geometric difficulties arising in dimensions 2 and 3. Building on our experience of writing the 1D scheme [20], a key ingredient consists in recasting a multidimensional Lagrangian scheme as a convex problem plus a skew-symmetric perturbation. Hereafter we propose a solution to treat the new difficulties that come from high dimension and we illustrate the fact that the series of iterative solves of the linear systems made of a coercive part plus a non trivial skew-symmetric part can be realized with standard libraries (PETSc [2] in our case).

An Eulerian scheme is easily derived by implementing an explicit ALE step after the implicit Lagrangian phase discussed in this work. Since an explicit ALE step is just a linear algorithm, it does not poses fundamental issues even if it can be very technical. One would obtain a scheme which is implicit with respect to the sound speed c and explicit with respect to the fluid velocity \mathbf{u} . The development of such an ALE method poses only minor technical issues, so we do not discuss them and focus on the main mathematical issues related to the Lagrangian phase.

The non-viscous multidimensional Euler system of compressible fluids endowed with an entropy inequality is

$$\left\{ \begin{array}{l} \partial_t \rho + \nabla \cdot (\rho \mathbf{u}) = 0, \\ \partial_t (\rho \mathbf{u}) + \nabla \cdot (\rho \mathbf{u} \otimes \mathbf{u}) + \nabla p = \mathbf{0}, \\ \partial_t (\rho E) + \nabla \cdot (\rho \mathbf{u} E + p \mathbf{u}) = 0, \\ \partial_t (\rho S) + \nabla \cdot (\rho S \mathbf{u}) \geq 0. \end{array} \right. \quad (1)$$

*CEA, DAM, DIF, F-91297 Arpajon, France and Université Paris-Saclay, LIHPC, France

†LJLL (UMR 7598) - Laboratoire Jacques-Louis Lions

‡Université Paris-Saclay, CEA, STMF, 91191, Gif-sur-Yvette, France

Here $\rho > 0$ denotes the density of the fluid, \mathbf{u} its velocity and E is the specific total energy. The pressure p is given as a function of the local thermodynamic state and can be expressed as a function of ρ and $e = E - \frac{1}{2}\langle \mathbf{u}, \mathbf{u} \rangle$, the specific internal energy. S is the physical specific entropy which satisfies the Gibbs relation $TdS = de + pd\tau$, where T is the temperature. For the sake of simplicity, in the paper we only consider perfect gas laws that is $p(\rho, e) = (\gamma - 1)\rho e$ with $\gamma > 1$. Extensions to more general complete equations of state are nearly straight-forward as soon as they are provided such that $\forall S \in \mathbb{R}, p_S : \tau \rightarrow p(\tau, S)$ is a strictly convex function and $\left. \frac{\partial p}{\partial \tau} \right|_S < 0$.

For our purposes it will be enough to consider the semi-Lagrangian formulation where $\tau = \frac{1}{\rho} > 0$ is the specific volume and $D_t = \partial_t + \mathbf{u} \cdot \nabla$ is the Lagrangian or material derivative

$$\begin{cases} \rho D_t \tau - \nabla \mathbf{u} = 0, \\ \rho D_t \mathbf{u} + \nabla p = \mathbf{0}, \\ \rho D_t E + \nabla \cdot (p \mathbf{u}) = 0, \\ \rho D_t S \geq 0. \end{cases} \quad (2)$$

An advantage of implicit schemes is that they are generally not subject to CFL-like conditions with regard to stability. However, they require the resolution of a nonlinear system. So the main mathematical issue is to understand under what conditions this nonlinear system admits a solution, and if the solution is unique. The second issue is of algorithmic nature. Indeed, even if the nonlinear system has a unique solution (something which is not guaranteed at all in the general case), it is necessary to develop an algorithm to solve and calculate this solution on a computer in a reliable manner. This is a topic which has been addressed many times in the literature. In this work, we will say the nonlinear system is well posed if there exists a unique solution of the nonlinear system for all time step $\Delta t > 0$. The construction of implicit and semi-implicit schemes for the Euler equations has always been considered as an important topic in the literature because it is a natural way to address low Mach flows [16, 4, 23]. A finite difference algorithm is proposed in [3], or implicit upwind methods are experimented in [26, 21]. A large number of references define predictor-corrector-like methods (see for instance [15] or [28]). In more recent works, implicit schemes are developed after relaxation as in [1] or [24]. In the context of our study, an important reference is [12], where an implicit Lagrangian scheme is examined for non-viscous compressible gas dynamics in 1D, but only by means of numerical experiments and without further theoretical foundation. Indeed, major technical difficulties appear for the resolution of fully implicit nonlinear schemes. At a theoretical level, it is difficult to prove existence and uniqueness of a solution for such schemes. Some strategies arise, among them the topological degree [13], or the use of the symmetrical structure of the linear part of the system as in [5].

Our contribution to implicit Lagrangian schemes in dimension $d \geq 2$ is based on a generalization of our recent work [20] restricted to dimension $d = 1$. We shall see that after algebraic manipulations, the proposed multidimensional extension of the scheme enters the theoretical framework that we already developed. More precisely: the scheme is well defined whichever the dimension is. Moreover it is unconditionally stable with regard to the time step. Indeed, providing at time t^n a physical state (for each cell j , $\tau_j^n > 0$ and $p_j^n > 0$), then the scheme computes a unique solution that satisfies $\tau_j^{n+1} > 0$ and $p_j^{n+1} > 0$ whatever the time step $t^{n+1} - t^n > 0$ is. Additionally, the scheme is entropy stable in the sense that $\forall j, S(\tau_j^{n+1}, e_j^{n+1}) \geq S(\tau_j^n, e_j^n)$.

We also discuss an important theoretical issue which is linked to the fact there are two natural ways to compute the volume V_j of a cell j . Firstly by stating that it is a function of the positions of the vertices r that define the cell

$$V_j(t) = V_j((\mathbf{x}_r(t))_r). \quad (3)$$

Secondly by integrating the continuity equation (first equation of (2)), which gives for a finite volume like method, the volume variation in time

$$V_j'(t) = \int_{\partial j(t)} \mathbf{u}(t) \cdot \mathbf{n}(t). \quad (4)$$

In dimension $d = 1$, both methods provide the same result so there is no issue. In dimension $d > 1$, both approaches give the same value for the continuous in time scheme and they also give almost the same value for explicit schemes for which the time step is restricted by the CFL stability condition.

However this is no more true for implicit schemes in general dimension with a large time step. This volume difference may yield instability of the scheme when data is recomputed according to the new volume given by (3). Our contribution to the solution of this issue in dimensions $2 \leq d \leq 3$ will be a specific algorithm to restore the equality of the volumes computed by (3) and (4). This will be obtained by using a special way of approximating the boundary integral in (4).

The organization of this work is as follows. In Section 2, we recall the main 1D results. We discretize the 1D isentropic Euler equations and explain how to write the scheme under the form (10). Section 2 also gives the ingredients of the proof of existence and uniqueness of a solution to the implicit scheme whose complete version can be found in [20]. In Section 3, we discretize (2) in semi-Lagrangian setting by using common notations issued from [9, 17] combined with the isentropic prediction [7]. We show that the isentropic implicit semi-Lagrangian scheme is endowed with the mathematical structure (10). Therefore it is a well posed system and it ensures that the isentropic implicit semi-Lagrangian scheme is also well posed. Section 3.3 is dedicated to a precise description of the volume difference issue that is introduced above. We explain how it can be cured, defining a practicable scheme that is unconditionally stable with regard to the time step. In Section 5 we explain how this implicit scheme naturally couples with the explicit one. This is an important feature since it provides a lot of flexibility and is of practical interest. Some numerical tests are presented in Section 6. We provide additional technical material on how we implement the numerical method.

Remark 1 (Boundary conditions). *We deliberately omit boundary conditions to keep the discussion as simple as possible and to focus on the main ingredients of the method. Actually, the treatment of boundary conditions may be a bit technical to implement but presents no specific difficulty. Classically with regard to Lagrangian methods, it consists more or less in imposing directly the values of the numerical fluxes or to deal with ghost cells when imposing symmetries or sliding to a straight wall (see [6]). Implicit boundary conditions treatment for these implicit schemes have been described and analyzed in [19].*

2 Structure of the 1D scheme

Before writing the multidimensional implicit discretization of (2) in the next Section, we remind the main mathematical observation which is to rewrite the implicit scheme (6)-(7) as a minimization problem plus a skew symmetric perturbation (10).

Starting from the 1D isentropic Euler equations

$$\begin{cases} \rho D_t \tau - \partial_x u = 0, \\ \rho D_t u + \partial_x p = 0, \\ \rho D_t S = 0, \end{cases} \quad (5)$$

consider a mesh M composed of N cells noted $j \in \{1, \dots, N\}$. The collection of cells is denoted $\mathcal{J} \ni j$ and the mass of cell j is M_j . Let us also introduce the notation \mathcal{R} which designates the set of all vertices or nodes of the mesh. For a cell $j \in \mathcal{J}$, we define the set of its nodes by $\mathcal{R}_j = \{j - \frac{1}{2}, j + \frac{1}{2}\}$. We write a predictor-corrector scheme followed by the mesh motion, so the algorithm is fundamentally made of 3 steps.

i) The implicit **prediction step** reads

$$\forall j \in \mathcal{J}, \quad \begin{cases} \bar{\tau}_j = \tau_j^n + \frac{\Delta t}{M_j} (\bar{u}_{j+\frac{1}{2}} - \bar{u}_{j-\frac{1}{2}}), \\ \bar{u}_j = u_j^n - \frac{\Delta t}{M_j} (\bar{p}_{j+\frac{1}{2}} - \bar{p}_{j-\frac{1}{2}}), \\ \bar{S}_j = S_j^n, \end{cases} \quad (6)$$

where the implicit fluxes $\bar{p}_{j+\frac{1}{2}}$ and $\bar{u}_{j+\frac{1}{2}}$ satisfy

$$\forall j + \frac{1}{2} \in \mathcal{R}, \quad \begin{cases} \bar{p}_{j+\frac{1}{2}} = \frac{\alpha_{j+\frac{1}{2}}}{2} (\bar{u}_j - \bar{u}_{j+1}) + \frac{1}{2} (\bar{p}_j + \bar{p}_{j+1}), \\ \bar{u}_{j+\frac{1}{2}} = \frac{1}{2\alpha_{j+\frac{1}{2}}} (\bar{p}_j - \bar{p}_{j+1}) + \frac{1}{2} (\bar{u}_j + \bar{u}_{j+1}), \end{cases} \quad (7)$$

and where $\alpha_{j+\frac{1}{2}} := \frac{1}{2}(\rho_j c_j + \rho_{j+1} c_{j+1}) > 0$. For simplicity of 1D notations, the definition of the fluxes corresponds here to the one state solver because the impedance at interface $x_{j+\frac{1}{2}}^n$ is shared by the two neighboring cells j and $j+1$. In practice one prefers to use two different values of the impedance (that is $\rho_j c_j$ and $\rho_{j+1} c_{j+1}$) in a more elaborate flux (thus denoted as a two states solver in [11]). A generic flux which incorporates such more elaborated use of acoustic impedance will be proposed in the multidimensional Section below.

ii) The explicit **correction step** is then obtained, after injection of the fluxes computed in the prediction step

$$\forall j \in \mathcal{J}, \quad \begin{cases} \tau_j^{n+1} = \tau_j^n + \frac{\Delta t}{M_j} (\overline{u_{j+\frac{1}{2}}} - \overline{u_{j-\frac{1}{2}}}), \\ u_j^{n+1} = u_j^n - \frac{\Delta t}{M_j} (\overline{p_{j+\frac{1}{2}}} - \overline{p_{j-\frac{1}{2}}}), \\ E_j^{n+1} = E_j^n - \frac{\Delta t}{M_j} (\overline{p_{j+\frac{1}{2}}} \overline{u_{j+\frac{1}{2}}} - \overline{p_{j-\frac{1}{2}}} \overline{u_{j-\frac{1}{2}}}). \end{cases} \quad (8)$$

iii) For **mesh motion**, the new node coordinates are given by

$$\forall j + \frac{1}{2} \in \mathcal{R}, \quad x_{j+\frac{1}{2}}^{n+1} = x_{j+\frac{1}{2}}^n + \Delta t \overline{u_{j+\frac{1}{2}}}. \quad (9)$$

The system (6)–(7) is a discretization of (5) which is considered as a prediction. One also notes that the correction step consists simply in restoring the conservation of total energy ($\tau^{n+1} = \bar{\tau}$ and $u^{n+1} = \bar{u}$ are unchanged from the prediction step).

The analysis of the entire loop (6-7-8-9) follows the structure of the method, that is we analyze the predictor step, then the corrector step, and finally the mesh motion.

2.1 The prediction step (6)–(7)

In [20], we have developed a general mathematical tool to show that the prediction scheme (6)–(7) is well posed. It relies on rewriting a given implicit nonlinear system under the form

$$\nabla J(U) = AU, \quad (10)$$

where U is the vector of unknowns, J is a strictly convex function which encodes both the physics of the problem and the numerical viscosity of the scheme, and finally A is a given skew-symmetric matrix which encodes the operator ∂_x in dimension one.

To fix ideas, in the case of the 1D implicit scheme (6)–(7), one has

$$U = \begin{pmatrix} (-\overline{p_j})_{j \in \mathcal{J}} \\ (\overline{\mathbf{u}_j})_{j \in \mathcal{J}} \end{pmatrix}. \quad (11)$$

The mathematical structure of (10) is the one of a minimization problem with a skew-symmetric perturbation. The proof that (10) is well posed is in [20]. It says that there always exists a unique solution under minor conditions which are fulfilled in our case. We provide the main steps of the next Proposition as an introduction for the multidimensional extension.

Proposition 1 ([20]). *The prediction step (6)–(7), or isentropic scheme, can be written under the form (10).*

Proof. As the entropy S is constant in (6)–(7), we omit its equation in the calculations. We replace the fluxes in (6) with their explicit formula (7). For all $j \in \mathcal{J}$ one has

$$\begin{cases} \overline{\tau_j} = \tau_j^n + \frac{\Delta t}{M_j} \left[\frac{1}{2\alpha_{j+\frac{1}{2}}} (\overline{p_j} - \overline{p_{j+1}}) + \frac{1}{2} (\overline{u_j} - \overline{u_{j+1}}) - \frac{1}{2\alpha_{j-\frac{1}{2}}} (\overline{p_{j-1}} - \overline{p_j}) - \frac{1}{2} (\overline{u_{j-1}} + \overline{u_j}) \right], \\ \overline{u_j} = u_j^n - \frac{\Delta t}{M_j} \left[\frac{\alpha_{j+\frac{1}{2}}}{2} (\overline{u_j} - \overline{u_{j+1}}) + \frac{1}{2} (\overline{p_j} + \overline{p_{j+1}}) - \frac{\alpha_{j-\frac{1}{2}}}{2} (\overline{u_{j-1}} - \overline{u_j}) - \frac{1}{2} (\overline{p_{j-1}} - \overline{p_j}) \right]. \end{cases} \quad (12)$$

Since during the prediction step the entropy is constant, the variable τ can be expressed in terms of the pressure¹ only, namely $\tau_j = \tau(-p_j)$. For the first line, we place on the left hand side the pressure depending terms and on the right hand side the ones depending on the velocity. We do the opposite for the second line.

$$\begin{cases} \bar{\tau}_j - \tau_j^n + \frac{\Delta t}{M_j} \left[\frac{1}{2\alpha_{j+\frac{1}{2}}}(\bar{p}_j - \bar{p}_{j+1}) - \frac{1}{2\alpha_{j-\frac{1}{2}}}(\bar{p}_{j-1} - \bar{p}_j) \right] = \frac{\Delta t}{M_j} \left(\frac{1}{2}(\bar{u}_j + \bar{u}_{j+1}) - \frac{1}{2}(\bar{u}_{j-1} + \bar{u}_j) \right), \\ \bar{u}_j - u_j^n - \frac{\Delta t}{M_j} \left[\frac{\alpha_{j+\frac{1}{2}}}{2}(\bar{u}_j - \bar{u}_{j+1}) - \frac{\alpha_{j-\frac{1}{2}}}{2}(\bar{u}_{j-1} - \bar{u}_j) \right] = -\frac{\Delta t}{M_j} \left(\frac{1}{2}(\bar{p}_j + \bar{p}_{j+1}) - \frac{1}{2}(\bar{p}_{j-1} - \bar{p}_j) \right). \end{cases} \quad (13)$$

We rearrange the terms and simplify the expressions to get

$$\begin{cases} \frac{M_j}{\Delta t}(\bar{\tau}_j - \tau_j^n) + \frac{1}{2\alpha_{j+\frac{1}{2}}}(\bar{p}_j - \bar{p}_{j+1}) + \frac{1}{2\alpha_{j-\frac{1}{2}}}(\bar{p}_j - \bar{p}_{j-1}) = -\frac{1}{2}\bar{u}_{j-1} + \frac{1}{2}\bar{u}_{j+1}, \\ \frac{M_j}{\Delta t}(\bar{u}_j - u_j^n) + \frac{\alpha_{j+\frac{1}{2}}}{2}(\bar{u}_j - \bar{u}_{j+1}) + \frac{\alpha_{j-\frac{1}{2}}}{2}(\bar{u}_j - \bar{u}_{j-1}) = \frac{1}{2}\bar{p}_{j-1} - \frac{1}{2}\bar{p}_{j+1}. \end{cases} \quad (14)$$

We define from there the objects of the formulation (10). The vector of unknowns in (10) is given by (11). In the case of a perfect gas law², the convex functional is $J : \mathcal{D} \rightarrow \mathbb{R}$, where $\mathcal{D} =]-\infty, 0[^N \times \mathbb{R}^N$ and

$$J(U) = \sum_{j=1}^N \frac{M_j}{\Delta t} [L_j^1(-p) + L_j^2(u)] + \sum_{j+\frac{1}{2} \in \mathcal{R}} [Q_{j+\frac{1}{2}}^1((-p_j)_{j \in \mathcal{J}}) + Q_{j+\frac{1}{2}}^2((u_j)_{j \in \mathcal{J}})]. \quad (15)$$

The elementary function L_j^1 depends on the equation of state of the fluid. In the case of perfect gases, one has for all $j \in \mathcal{J}$

$$L_j^1 : \mathbb{R}^- \rightarrow \mathbb{R}, \quad L_j^1(-p) = -p^{1-\frac{1}{\gamma}} \gamma (\gamma - 1)^{\frac{1}{\gamma}-1} \exp\left(\frac{S}{C_v}\right)^{\frac{1}{\gamma}} + \tau_j^n p, \quad (16)$$

with C_v the thermal capacity at constant volume. For all $j \in \mathcal{J}$

$$L_j^2 : \mathbb{R} \rightarrow \mathbb{R}, \quad L_j^2(u) = \frac{u^2}{2} - u u_j^n. \quad (17)$$

The functions $Q_{j+\frac{1}{2}}^1$ and $Q_{j+\frac{1}{2}}^2$ depend on the choice of the scheme via the definition of the fluxes. For all $j \in \mathcal{J}$,

$$Q_{j+\frac{1}{2}}^1((-p_j)_{j \in \mathcal{J}}) = \frac{1}{2\alpha_{j+\frac{1}{2}}} \frac{(p_j - p_{j+1})^2}{2}, \quad (18)$$

and

$$Q_{j+\frac{1}{2}}^2((u_j)_{j \in \mathcal{J}}) = \frac{\alpha_{j+\frac{1}{2}}}{2} \frac{(u_j - u_{j+1})^2}{2}. \quad (19)$$

The skew-symmetric matrix is $A \in \mathcal{M}_{2N}(\mathbb{R})$. With periodic boundary conditions, it is of the form

$$A = \frac{1}{2} \begin{bmatrix} 0 & B \\ -B^T & 0 \end{bmatrix} \quad \text{with} \quad B = \begin{bmatrix} 0 & 1 & 0 & \cdots & 0 & -1 \\ -1 & 0 & 1 & 0 & \cdots & 0 \\ 0 & \ddots & \ddots & \ddots & \ddots & \vdots \\ \vdots & \ddots & \ddots & \ddots & \ddots & 0 \\ 0 & \cdots & 0 & -1 & 0 & 1 \\ 1 & 0 & \cdots & 0 & -1 & 0 \end{bmatrix} \in \mathcal{M}_N(\mathbb{R}). \quad (20)$$

□

¹During the prediction step $p_j(t) = p(\tau_j(t), S_j^n) = p_{S_j^n}(\tau_j(t))$, thus as soon as $p_{S_j^n}$ is a strictly decreasing function of τ , one can write $\tau_j = \tau(-p_j)$. This is the case for many equations of state, and obviously for perfect gases.

²For other equations of states, the domain of definition \mathcal{D} of J itself is likely to change.

Theorem 1 ([20]). *Consider the problem (10) where U , J and A are respectively defined by (11), (15) and (20). Assume that $U^n \in \mathcal{D}$. Then (10) has a unique solution $U \in \mathcal{D} =]-\infty, 0[^N \times \mathbb{R}^N$.*

Proof. The proof of uniqueness relies on elementary considerations. Assume that (10) admits a solution. Let $U_1 \in \mathcal{D}$ and $U_2 \in \mathcal{D}$ be two solutions of the problem (10), namely

$$\begin{cases} \nabla J(U_1) = AU_1, \\ \nabla J(U_2) = AU_2. \end{cases}$$

One has

$$\langle \nabla J(U_1) - \nabla J(U_2), U_1 - U_2 \rangle = \langle A(U_1 - U_2), U_1 - U_2 \rangle.$$

Since A is a skew-symmetric matrix, therefore $\langle A(U_1 - U_2), U_1 - U_2 \rangle = 0$. It means

$$\langle \nabla J(U_1) - \nabla J(U_2), U_1 - U_2 \rangle = 0.$$

Since J is strictly convex, this is only satisfied if $U_1 = U_2$, which concludes the uniqueness of a solution.

The existence of a solution is tougher than the uniqueness. We only mention the important steps and the interested reader can find all the details in [20]. We first prove that there exists a minimum point for J inside of \mathcal{D} . It is a classical result in convex analysis and is based on Theorem 27.1 (d) p 265 of Rockafellar [27]. Then, we rewrite the scheme under the form of a family of Cauchy problems with a parameter ε that varies between 0 (convex minimization problem) and 1 (the principal problem). We prove that this problem

$$\begin{cases} \text{Find } U_\varepsilon \in \mathcal{D} \text{ such that} \\ \nabla J(U_\varepsilon) = \varepsilon AU_\varepsilon, \end{cases} \quad (21)$$

admits a solution. Finally, using bounds we conclude on the existence of a solution for the prediction scheme for all $\Delta t > 0$. \square

Observe that since the solution of the prediction scheme is unique and belongs to \mathcal{D} , a direct consequence is that, $\forall j \in \mathcal{J}$, $\bar{p}_j > 0$. It implies immediately that $\forall j \in \mathcal{J}$, $\bar{\tau}_j > 0$ and $\bar{\rho}_j > 0$. This is an important stability result. However, one can prove an additional stability result: mathematical entropy associated to (5) decreases under the action of the prediction step. Actually, following [7] the total energy E is an entropy for isentropic Euler equations (5)

$$\partial_t(\rho E) + \partial_x(\rho u E) + \partial_x(pu) \leq 0, \quad (22)$$

or in the semi-Lagrangian setting

$$\rho D_t E + \partial_x(pu) \leq 0. \quad (23)$$

In [20], we showed that the solution of the predictor step satisfies

$$\forall j \in \mathcal{J}, \quad \frac{\bar{E}_j - E_j^n}{\Delta t} + \frac{\bar{p}_{j+\frac{1}{2}} \bar{u}_{j+\frac{1}{2}} - \bar{p}_{j-\frac{1}{2}} \bar{u}_{j-\frac{1}{2}}}{M_j} \leq 0. \quad (24)$$

This is a second and important stability result. It is of fundamental use to prove that the overall scheme is entropy stable $\forall j \in \mathcal{J}$, $S_j^{n+1} \geq S_j^n$, see Section 2.2.

Let us mention a few additional features. First, the scheme (6)–(7) is conservative in mass, volume, momentum and entropy. Second, it is Galilean invariant. To solve the implicit scheme, a Newton algorithm is used. Numerical 1D illustrations are provided in [20], and show that the theoretical properties of unconditional robustness transfer to real calculations. In practice, the Newton algorithm converges in few iterations. We have observed a maximum of 7 iterations in 1D for very large CFL numbers (>100).

2.2 The correction step (8)

An extremely important property is that the correction step is explicit, so computationally very cheap, and it is nevertheless unconditionally stable.

One has by construction that $\tau_j^{n+1} = \bar{\tau}_j > 0$. Moreover, as the prediction step is entropic (24) in the mathematical sense, then the specific total energy (8) satisfies the following inequality

$$\forall j \in \mathcal{J}, \quad E_j^{n+1} \geq \bar{E}_j.$$

Therefore, since one has $u_j^{n+1} = \bar{u}_j$, specific internal energies are ordered the same way

$$\forall j \in \mathcal{J}, \quad e_j^{n+1} \geq \bar{e}_j.$$

Finally, because the specific volume is unchanged during the correction step and since Gibbs relation implies that $\frac{\partial S}{\partial e}|_\tau = \frac{1}{T} > 0$, S is an increasing function of e and one gets

$$\forall j \in \mathcal{J}, \quad S_j^{n+1} = S(\tau_j^{n+1}, e_j^{n+1}) = S(\bar{\tau}_j, e_j^{n+1}) \geq S(\bar{\tau}_j, \bar{e}_j) = \bar{S}_j = S_j^n.$$

In other words the complete scheme produces physical entropy $\forall \Delta t > 0$. This sole property explains that the correction step is stable for all time step. Once again this is a striking feature since the correction step is explicit.

2.3 The mesh motion (9)

At the beginning of the time step the mesh is correct: the local volume is positive $V_j^n = x_{j+\frac{1}{2}}^n - x_{j-\frac{1}{2}}^n > 0$ and the mass in the cell is $M_j = V_j^n \rho_j^n > 0$. The issue is to insure the correctness of the mesh after the mesh motion (9). It appears that this is guaranteed without further conditions.

Indeed the equation for the calculation of $\tau_j^{n+1} = \bar{\tau}_j$ can be combined with the mesh displacement (9) to obtain

$$M_j \tau_j^{n+1} = M_j \tau_j^n + \left(x_{j+\frac{1}{2}}^{n+1} - x_{j-\frac{1}{2}}^{n+1} \right) - \left(x_{j+\frac{1}{2}}^n - x_{j-\frac{1}{2}}^n \right) = V_j^n + V_j^{n+1} - V_j^n = V_j^{n+1} = x_{j+\frac{1}{2}}^{n+1} - x_{j-\frac{1}{2}}^{n+1}.$$

Since it was already proved that $\tau_j^{n+1} > 0$, and M_j is conserved in semi-Lagrangian, it implies that

$$x_{j+\frac{1}{2}}^{n+1} - x_{j-\frac{1}{2}}^{n+1} > 0.$$

This inequality explains that the mesh displacement step of our method is stable in 1D without CFL condition.

3 Extension to higher dimensions

In this section, we explain how to adapt the strategy described above to define implicit Lagrangian schemes in higher dimensions. A new difficulty related to the evolution of the cells geometry has to be overcome to chain time steps. To do so, a particular attention will be brought to the management of geometrical quantities appearing in the scheme in Section 3.3.

To define a multidimensional semi-Lagrangian finite volume scheme, we combine two ideas. The first one is to use the nodal solver framework introduced in [18, 10] to write multidimensional implicit versions of Glace [6] or Eucclhyd [17, 14] schemes. The second idea is to use the same time discretization as the one we proposed in [20]: a nonlinear implicit isentropic predictor scheme, followed by an explicit corrector which reestablishes the total energy conservation.

Let us remind the general structure of these nodal solvers in arbitrary dimension of space. The continuous in time scheme family reads in dimension d ,

$$\forall j \in \mathcal{J}, \quad \begin{cases} M_j \tau_j' = \sum_{r \in \mathcal{R}_j} \langle \mathbf{C}_{jr}, \mathbf{u}_r \rangle, \\ M_j \mathbf{u}_j' = - \sum_{r \in \mathcal{R}_j} \mathbf{F}_{jr}, \\ M_j E_j' = - \sum_{r \in \mathcal{R}_j} \langle \mathbf{F}_{jr}, \mathbf{u}_r \rangle, \end{cases} \quad (25)$$

where at each node r , \mathbf{F}_{jr} and \mathbf{u}_r are solutions of the local linear systems

$$\forall r \in \mathcal{R}, \quad \begin{cases} \forall j \in \mathcal{J}_r, & \mathbf{F}_{jr} = A_{jr}(\mathbf{u}_j - \mathbf{u}_r) + \mathbf{C}_{jr}p_j, \\ \text{and} & \sum_{j \in \mathcal{J}_r} \mathbf{F}_{jr} = \mathbf{0}, \end{cases} \quad (26)$$

and where the \mathbf{C}_{jr} vectors satisfy the two following properties

$$\forall j \in \mathcal{J}, \quad \sum_{r \in \mathcal{R}_j} \mathbf{C}_{jr} = \mathbf{0}, \quad \text{and} \quad \forall r \in \mathcal{R}, \quad \sum_{j \in \mathcal{J}_r} \mathbf{C}_{jr} = \mathbf{0}. \quad (27)$$

The scheme is correctly defined as soon as $A_r = \sum_{j \in \mathcal{J}_r} A_{jr} > 0$ (for all $r \in \mathcal{R}$) are symmetric positive matrices which is the case on non-degenerate meshes. It is easy to show that the scheme is conservative in mass, volume, momentum and total energy. Also, as soon as A_{jr} matrices are non negative, the scheme is entropy stable. The weak consistency is established in [9] for the generic choice

$$\forall j \in \mathcal{J}, \forall r \in \mathcal{R}_j, \quad \mathbf{C}_{jr} := \nabla_{\mathbf{x}_r} V_j. \quad (28)$$

Denote by \mathcal{F}_j and \mathcal{F}_r the sets of faces connected respectively to the cell j and to the node r . Thus \mathbf{N}_{jfr} is the gradient of variation of the cell j with regard to the position of r associated to the face f . One has $\sum_{f \in \mathcal{F}_j \cap \mathcal{F}_r} \mathbf{N}_{jfr} = \mathbf{C}_{jr}$. These notations are enough to describe two popular methods which are the Glace scheme and the Eucclhyd scheme

$$A_{jr}^G := \rho_j c_j \frac{\mathbf{C}_{jr} \otimes \mathbf{C}_{jr}}{\|\mathbf{C}_{jr}\|}, \quad \text{and} \quad A_{jr}^E := \rho_j c_j \sum_{f \in \mathcal{F}_j \cap \mathcal{F}_r} \frac{\mathbf{N}_{jfr} \otimes \mathbf{N}_{jfr}}{\|\mathbf{N}_{jfr}\|}. \quad (29)$$

Both choice yield that $A_r := \sum_{j \in \mathcal{J}_r} A_{jr} > 0$ are positive definite in standard conditions. The acoustic impedance is local in the sense that it is calculated cell-wise, which corresponds to a generic two states flux in [11]. Then mimicking the 1D scheme, we write a 3 steps scheme where the first two steps are the predictor-corrector part.

i) The implicit **prediction step** structure is

$$\forall j \in \mathcal{J}, \quad \begin{cases} \bar{\tau}_j = \tau_j^n + \frac{\Delta t}{M_j} \sum_{r \in \mathcal{R}_j} \langle \mathbf{D}_{jr}, \bar{\mathbf{u}}_r \rangle, \\ \bar{\mathbf{u}}_j = \mathbf{u}_j^n - \frac{\Delta t}{M_j} \sum_{r \in \mathcal{R}_j} \bar{\mathbf{F}}_{jr}, \\ \bar{S}_j = S_j^n, \end{cases} \quad (30)$$

where the numerical fluxes are given by

$$\forall r \in \mathcal{R}, \quad \begin{cases} \forall j \in \mathcal{J}_r, & \bar{\mathbf{F}}_{jr} = A_{jr}(\bar{\mathbf{u}}_j - \bar{\mathbf{u}}_r) + \mathbf{D}_{jr} \bar{p}_j, \\ \text{and} & \sum_{j \in \mathcal{J}_r} \bar{\mathbf{F}}_{jr} = \mathbf{0}. \end{cases} \quad (31)$$

The vectors \mathbf{D}_{jr} are the geometrical vectors used to represent the influence of the mesh. A natural choice is of course to take the explicit value $\mathbf{D}_{jr} = \mathbf{C}_{jr}^n$. However it will be obvious later that the explicit value is not the best theoretical choice. This is why we use this notation and postpone the exact definition of these vectors.

ii) Then the explicit **correction step** reads as

$$\forall j \in \mathcal{J}, \quad \begin{cases} \tau_j^{n+1} = \tau_j^n + \frac{\Delta t}{M_j} \sum_{r \in \mathcal{R}_j} \langle \mathbf{D}_{jr}, \bar{\mathbf{u}}_r \rangle, \\ \mathbf{u}_j^{n+1} = \mathbf{u}_j^n - \frac{\Delta t}{M_j} \sum_{r \in \mathcal{R}_j} \bar{\mathbf{F}}_{jr}, \\ E_j^{n+1} = E_j^n - \frac{\Delta t}{M_j} \sum_{r \in \mathcal{R}_j} \langle \bar{\mathbf{F}}_{jr}, \bar{\mathbf{u}}_r \rangle, \end{cases} \quad (32)$$

with the same vectors \mathbf{D}_{jr} .

iii) The **mesh motion** is defined by

$$\forall r \in \mathcal{R}, \quad \mathbf{x}_r^{n+1} = \mathbf{x}_r^n + \Delta t \bar{\mathbf{u}}_r. \quad (33)$$

All the difficulties to solve this coupled problem come from the implicit step (30)–(31) that corresponds to the discretization of the isentropic Euler equations.

3.1 The prediction step (30)–(31)

To prove that the implicit predictor step (30)–(31) is correctly defined and admits a unique solution, it is recast as a perturbed minimization problem [20] of the form (10). To ease the analysis and the further implementation, the various terms are written within an abstract vector-matrix form.

Proposition 2. *The implicit scheme (30)–(31) can be written under the form (10).*

Proof. To formalize the implicit prediction step, we want to substitute $\bar{\mathbf{F}}_{jr}$ and $\bar{\mathbf{u}}_r$ by their expressions in terms of $\bar{\mathbf{u}}_j$ and $\bar{\mathbf{p}}_j$ into (30). One computes the expression of $\bar{\mathbf{u}}_r$ by injecting the first equation of (31) into the second. One gets

$$\forall r \in \mathcal{R}, \quad \bar{\mathbf{u}}_r = A_r^{-1} \sum_{j \in \mathcal{J}_r} A_{jr} \bar{\mathbf{u}}_j + A_r^{-1} \sum_{j \in \mathcal{J}_r} \mathbf{D}_{jr} \bar{p}_j. \quad (34)$$

One substitutes this value in the first equation of (31). It gives

$$\forall j \in \mathcal{J}, \forall r \in \mathcal{R}_j, \quad \bar{\mathbf{F}}_{jr} = A_{jr} \left(\bar{\mathbf{u}}_j - \left(A_r^{-1} \sum_{i \in \mathcal{J}_r} A_{ir} \bar{\mathbf{u}}_i + A_r^{-1} \sum_{i \in \mathcal{J}_r} \mathbf{D}_{ir} \bar{p}_i \right) \right) + \mathbf{D}_{jr} \bar{p}_j. \quad (35)$$

Then one injects (34) and (35) into (30), omitting the trivial entropy conservation equation. It reads

$$\forall j \in \mathcal{J}, \quad \begin{cases} \bar{\tau}_j = \tau_j^n + \frac{\Delta t}{M_j} \sum_{r \in \mathcal{R}_j} \left\langle \mathbf{D}_{jr}, A_r^{-1} \bar{\mathbf{u}}_i + A_r^{-1} \sum_{i \in \mathcal{J}_r} \mathbf{D}_{ir} \bar{p}_i \right\rangle, \\ \bar{\mathbf{u}}_j = \mathbf{u}_j^n - \frac{\Delta t}{M_j} \sum_{r \in \mathcal{R}_j} \left[A_{jr} \left(\bar{\mathbf{u}}_j - \left(A_r^{-1} \sum_{i \in \mathcal{J}_r} A_{ir} \bar{\mathbf{u}}_i + A_r^{-1} \sum_{i \in \mathcal{J}_r} \mathbf{D}_{ir} \bar{p}_i \right) \right) + \mathbf{D}_{jr} \bar{p}_j \right]. \end{cases} \quad (36)$$

A reorganization of the terms depending on the pressure on the one side and the ones depending on the velocity on the other side gives $\forall j \in \mathcal{J}$,

$$\begin{cases} \frac{M_j}{\Delta t} (\bar{\tau}_j - \tau_j^n) - \sum_{r \in \mathcal{R}_j} \langle \mathbf{D}_{jr}, A_r^{-1} \sum_{i \in \mathcal{J}_r} \mathbf{D}_{ir} \bar{p}_i \rangle = \sum_{r \in \mathcal{R}_j} \langle \mathbf{D}_{jr}, A_r^{-1} \sum_{i \in \mathcal{J}_r} A_{ir} \bar{\mathbf{u}}_i \rangle, \\ \frac{M_j}{\Delta t} (\bar{\mathbf{u}}_j - \mathbf{u}_j^n) - \sum_{r \in \mathcal{R}_j} A_{jr} A_r^{-1} \sum_{i \in \mathcal{J}_r} A_{ir} \bar{\mathbf{u}}_i + \sum_{r \in \mathcal{R}_j} A_{jr} \bar{\mathbf{u}}_j = - \sum_{r \in \mathcal{R}_j} \mathbf{D}_{jr} \bar{p}_j + \sum_{r \in \mathcal{R}_j} A_{jr} A_r^{-1} \sum_{i \in \mathcal{J}_r} \mathbf{D}_{ir} \bar{p}_i. \end{cases} \quad (37)$$

From this semi-abstract vector-matrix formulation, one deduces the definitions of the objects entering in (10). The vector of unknowns is $U \in \mathbb{R}^{N+dN}$

$$U = \begin{pmatrix} (-\bar{p}_j)_{j \in \mathcal{J}} \\ (\bar{\mathbf{u}}_j)_{j \in \mathcal{J}} \end{pmatrix}. \quad (38)$$

The skew-symmetric matrix is $A \in \mathcal{M}_{N+dN}(\mathbb{R})$

$$A = \begin{bmatrix} 0 & B \\ -B^T & 0 \end{bmatrix}, \quad (39)$$

where $B \in \mathcal{M}_N(\mathcal{M}_{1,d}(\mathbb{R}))$ is defined by

$$\forall i, j \in \mathcal{J}, \quad B_{ji} = \sum_{r \in \mathcal{R}_i \cap \mathcal{R}_j} (\mathbf{D}_{jr})^T A_r^{-1} A_{ir}. \quad (40)$$

The convex functional $J : \mathcal{D} \rightarrow \mathbb{R}$ is defined by

$$J(U) = \sum_{j=1}^N \frac{M_j}{\Delta t} [L_j^1(-p) + L_j^2(\mathbf{u})] + \sum_{r \in \mathcal{R}} \left[Q_r^1((-p_j)_{j \in \mathcal{J}}) + Q_r^2((\mathbf{u}_j)_{j \in \mathcal{J}}) \right] \quad (41)$$

where the functions L_j^1 , L_j^2 , Q_r^1 and Q_r^2 are given below.

In the case of a perfect gas law, the function L_j^1 is given by

$$L_j^1 : \mathbb{R}^- \rightarrow \mathbb{R}, \quad L_j^1(-p) = -p^{1-\frac{1}{\gamma}} (\gamma-1)^{\frac{1}{\gamma}-1} \gamma \exp\left(\frac{S_j^n}{C_v}\right)^{\frac{1}{\gamma}} + \tau_j^n p. \quad (42)$$

The function L_j^2 corresponds to

$$L_j^2 : \mathbb{R}^d \rightarrow \mathbb{R}, \quad L_j^2(\mathbf{u}) = \frac{\langle \mathbf{u}, \mathbf{u} \rangle}{2} - \langle \mathbf{u}_j^n, \mathbf{u} \rangle. \quad (43)$$

The function Q_r^1 is given by $Q_r^1 : \mathbb{R}^N \rightarrow \mathbb{R}$,

$$Q_r^1((-p_l)_{l \in \mathcal{J}}) = \frac{1}{2} \left\langle \sum_{j \in \mathcal{J}_r} \mathbf{D}_{jr}(-p_j), A_r^{-1} \sum_{j \in \mathcal{J}_r} \mathbf{D}_{jr}(-p_j) \right\rangle. \quad (44)$$

Finally one sets $Q_r^2 : \mathbb{R}^{dN} \rightarrow \mathbb{R}$,

$$Q_r^2((\mathbf{u}_l)_{l \in \mathcal{J}}) = \frac{1}{2} \sum_{j \in \mathcal{J}_r} \langle A_{jr} \mathbf{u}_j, \mathbf{u}_j \rangle - \frac{1}{2} \left\langle \sum_{j \in \mathcal{J}_r} A_{jr} \mathbf{u}_j, A_r^{-1} \sum_{j \in \mathcal{J}_r} A_{jr} \mathbf{u}_j \right\rangle. \quad (45)$$

□

Theorem 2. Assuming that $U^n \in \mathcal{D}$, then the problem (10) where U , J and A are respectively given by (38), (41) and (39) has a unique solution in $\mathcal{D} =]-\infty, 0[^N \times \mathbb{R}^{dN}$.

Proof. The proof is exactly the same as the one of Theorem 1. □

Since the unique solution of the isentropic implicit solver lives in \mathcal{D} , one gets $\forall j \in \mathcal{J}$, $\bar{p}_j > 0$ as in 1D. Thus as during this isentropic step τ is only a function of p , it ensures that $\bar{\tau}_j > 0$, therefore after the correction step one also gets

$$\forall j \in \mathcal{J}, \quad \tau_j^{n+1} = \bar{\tau}_j > 0.$$

It ensures that

$$\forall \Delta t > 0, \forall j \in \mathcal{J}, \quad \rho_j^{n+1} > 0.$$

As we already stated in Section 2, the specific total energy is a mathematical entropy for the isentropic Euler system (see [7]), in semi-Lagrangian coordinates, it writes

$$\rho D_t E + \nabla \cdot (p \mathbf{u}) \leq 0. \quad (46)$$

The predictor scheme (30)–(31) satisfies this inequality.

Proposition 3. The prediction scheme (30)–(31) satisfies the following inequality on total energy

$$\forall \Delta t > 0, \forall j \in \mathcal{J}, \quad M_j \frac{\bar{E}_j - E_j^n}{\Delta t} + \sum_{r \in \mathcal{R}_j} \langle \bar{\mathbf{F}}_{jr}, \bar{\mathbf{u}}_r \rangle \leq 0. \quad (47)$$

Proof. The proof follows the one given for the 1D case in [20] but requires a few technical but non essential adjustments. It is detailed in Appendix A. □

3.2 The correction step (32)

The last stability result establishes that the whole predictor-corrector scheme is entropy stable.

Proposition 4. *The correction scheme (32)–(31) is stable in the sense that it satisfies an entropy inequality*

$$\forall \Delta t > 0, \forall j \in \mathcal{J}, \quad \frac{S_j^{n+1} - S_j^n}{\Delta t} \geq 0. \quad (48)$$

Proof. The proof is exactly the same as in the 1D case, see Section 2.2. \square

We state a few important results that are more standard with regard to nodal solvers

Proposition 5 (Conservation). *The isentropic implicit scheme (30)–(31) is conservative in volume, mass, momentum and total energy.*

The whole implicit scheme (30)–(32) is conservative in volume, mass, momentum and total energy.

Proof. The proof is similar to the explicit case and is omitted here. \square

Additionally it is easy to check that the isentropic scheme (30)–(31) and the whole scheme (30)–(32) are Galilean invariant.

3.3 The mesh motion (33)

Mesh displacement in dimension $d > 1$ cannot be analyzed with the simple method of Section 2.3 which is specific to dimension $d = 1$. We do not know a comprehensive theoretical formulation of what is a correct mesh motion for any type of cells in dimension $d > 1$. That is why we focus on volume considerations which is already a guide to understand the issues at stake.

Suppose that the mesh moves at a given velocity \mathbf{u}_r for all $r \in \mathcal{R}$. Take the first equation in the continuous in time formulation (25)–(26). One can use $M_j = V_j(t)\rho_j(t)$ and write the variation in time of the volume as

$$V_j' = \sum_{r \in \mathcal{R}_j} \langle \mathbf{C}_{jr}, \mathbf{u}_r \rangle.$$

Starting from the velocities computed by the scheme, a first possibility to discretize this equation writes

$$\bar{V}_j = V_j^n + \Delta t \sum_{r \in \mathcal{R}_j} \langle \mathbf{C}_{jr}^n, \mathbf{u}_r \rangle. \quad (49)$$

A second possibility is to move the mesh with $\forall r \in \mathcal{R}, \quad \mathbf{x}_r^{n+1} = \mathbf{x}_r^n + \Delta t \mathbf{u}_r$ and then to calculate the new volumes. Since the volume is an homogeneous function of degree d , one can use for example the exact formula

$$V_j^{n+1} := \frac{1}{d} \sum_{r \in \mathcal{R}_j} \langle \mathbf{C}_{jr}^{n+1}, \mathbf{x}_r^{n+1} \rangle. \quad (50)$$

The question is: are the two volumes (49) and (50) actually equal? If they are equal one can reproduce the analysis made in Section 2.3 which ensures the positivity of the new volume after mesh displacement. If they are not equal we do not know how to continue the analysis. The important property is as follows.

Property 1. *One has the exact formula*

$$V_j^{n+1} - \bar{V}_j = \Delta t^2 \mathcal{G}_j, \quad (51)$$

where \mathcal{G}_j depends on the dimension d

$$\begin{cases} d = 1, & \mathcal{G}_j = 0, \\ d = 2, & \mathcal{G}_j = \frac{1}{2} \sum_{r \in \mathcal{R}_j} \langle \mathbf{u}_{r+1}^n, (\mathbf{u}_r^n)^\perp \rangle, \\ d = 3, & \mathcal{G}_j = \sum_{r \in \mathcal{R}_j} \sum_{f \in \mathcal{F}_{jr}} \frac{1}{12N_f} \left\langle \sum_{s \in \mathcal{R}_{jf}} \left(2[\mathbf{u}^n]_r^{jf} - [\mathbf{u}^n]_s^{jf} \right) \wedge \mathbf{u}_s^n, \mathbf{x}_r^n + \frac{\Delta t}{3} \mathbf{u}_r^n \right\rangle, \end{cases}$$

where the object $[[\cdot]]^{jf}$ in dimension $d = 3$ is introduced in Notation 1 at the end of this Section.

A corollary is that the volumes (49) and (50) are different in the general case in dimension $d \in \{2, 3\}$.

Proof. The result is already proved in dimension $d = 1$. The rest of the proof is technical and thus given in an Annex paper [8]. \square

The interpretation of (51) is that the two predictions of the volume provide a priori different results for $d > 1$. This feature of lagrangian volume calculations has been noticed by many researchers. For explicit schemes this is not a mere restriction since it is sufficient to take a CFL condition and a time step which is small enough. The difference is second order in time and (51) explains that the two methods of numerical integration will provide essentially the same result. However we consider implicit schemes in this work, and we do not desire to bound the time step with such considerations. In summary (51) explains that the difference of volumes is small for explicit schemes and can be a priori large for implicit schemes.

Remark 2 (Special case all dimensions). *If all nodal velocities of the cell j are colinear, then $\mathcal{G}_j = 0$ in (51) in all dimensions.*

Notation 1 (3D). *Let $j \in \mathcal{J}$ be a 3D cell of a mesh and $f \in \mathcal{F}_j$ be a face of j . We define the operator $[[\cdot]]^{jf}$ by*

$$\forall s \in \mathcal{R}_{jf}, \quad [[\phi]]_s^{jf} = \phi_{s+1} - \phi_{s-1},$$

where \mathcal{R}_{jf} is the ordered set of nodes of the face f . The order is set to define the normal to f outgoing from the cell j . The notation $s+1$ (resp. $s-1$) designates the node after (resp. before) the node s in \mathcal{R}_{jf} (see Figure 1).

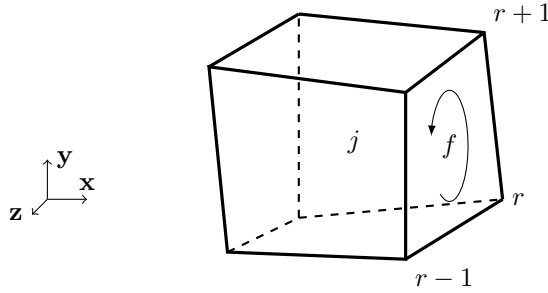


Figure 1: Illustration of the local node ordering with regard to a face of a cell. The ordering is locally defined by browsing the nodes r of the face f in the way that defines the normal outgoing from the cell j . This ordered set is denoted \mathcal{R}_{jf} .

3.4 Description of \mathbf{D}_{jr} vectors

To obtain the equality of volumes in (51) in all dimensions, we replace (50) with the new definition

$$\bar{V}_j = V_j^n + \Delta t \sum_{r \in \mathcal{R}_j} \langle \mathbf{D}_{jr}, \mathbf{u}_r \rangle \quad (52)$$

where the vectors \mathbf{D}_{jr} are some degrees of freedom. Our objective is to propose a suitable set of \mathbf{D}_{jr} vectors such that the equality of volumes is restored. In other words one wants to solve the following Problem.

Problem 1. *Find specific vectors $\mathbf{D}_{jr} \in \mathbb{R}^d$, for all $j \in \mathcal{J}$ and for all $r \in \mathcal{R}_j$, such that*

$$\forall j \in \mathcal{J}, \Delta t \sum_{r \in \mathcal{R}_j} \langle \mathbf{D}_{jr}, \mathbf{u}_r \rangle = \frac{1}{d} \sum_{r \in \mathcal{R}_j} \langle \mathbf{C}_{jr}^{n+1}, \mathbf{x}_r^{n+1} \rangle - \frac{1}{d} \sum_{r \in \mathcal{R}_j} \langle \mathbf{C}_{jr}^n, \mathbf{x}_r^n \rangle. \quad (53)$$

In this Problem, $\Delta t = t^{n+1} - t^n > 0$ and the grid velocity is defined by $\mathbf{u}_r = \frac{1}{\Delta t}(\mathbf{x}_r^{n+1} - \mathbf{x}_r^n)$. In the construction of the solution of this problem, we add the conditions

$$\forall j \in \mathcal{J}, \sum_{r \in \mathcal{R}_j} \mathbf{D}_{jr} = \mathbf{0}, \quad \text{and} \quad \forall r \in \mathcal{R}, \sum_{j \in \mathcal{J}_r} \mathbf{D}_{jr} = \mathbf{0} \quad (54)$$

because they are already mesh conditions naturally satisfied by \mathbf{C}_{jr}^n .

Proposition 6. *Problem (1) admits a unique solution.*

- In dimension $d = 1$,

$$\forall j \in \mathcal{J}, \quad D_{j,j \pm \frac{1}{2}} = \pm 1. \quad (55)$$

- In dimension $d = 2$,

$$\forall j \in \mathcal{J}, \forall r \in \mathcal{R}_j, \quad \mathbf{D}_{jr} = \frac{1}{2} (\mathbf{C}_{jr}^n + \mathbf{C}_{jr}^{n+1}), \quad (56)$$

where $\mathbf{C}_{jr}^n = -\frac{1}{2}(\mathbf{x}_{r+1}^n - \mathbf{x}_{r-1}^n)^\perp$.

- In dimension $d = 3$,

$$\forall j \in \mathcal{J}, \forall r \in \mathcal{R}_j, \quad \mathbf{D}_{jr} = \frac{1}{2} (\mathbf{C}_{jr}^n + \mathbf{C}_{jr}^{n+1}) + \mathbf{C}_{jr}^\delta, \quad (57)$$

where $\mathbf{C}_{jr}^n = \sum_{f \in \mathcal{F}_{jr}} \frac{1}{12N_f} \left(\sum_{s \in \mathcal{R}_{jf}} (2[\mathbf{x}]_r^{jf^n} - [\mathbf{x}]_s^{jf^n}) \wedge \mathbf{x}_s^n \right)$ and

$$\mathbf{C}_{jr}^\delta = - \sum_{f \in \mathcal{F}_{jr}} \frac{1}{12N_f} \sum_{s \in \mathcal{R}_{jf}} \frac{1}{6} \left[2([\mathbf{x}]_r^{jf^{n+1}} - [\mathbf{x}]_r^{jf^n}) - ([\mathbf{x}]_s^{jf^{n+1}} - [\mathbf{x}]_s^{jf^n}) \right] \wedge (\mathbf{x}_s^{n+1} - \mathbf{x}_s^n).$$

A corollary is that the volumes (49) and (52) are equal in all dimensions.

Proof. The proof is calculative especially in 3D. Thus, for the sake of clarity, it is also given in the Annex paper [8]. \square

4 Detailed algorithm

Since the vectors \mathbf{D}_{jr} must be calculated as well, we introduce them in the predictor step with a fixed point method. One obtains the Algorithm below.

Full Algorithm

Initialization: All quantities are known at time t^n .

- Define initial guess for \mathbf{D}_{jr} : $\forall j \in \mathcal{J}, \forall r \in \mathcal{R}_j, \quad \mathbf{D}_{jr}^{n,0} := \mathbf{C}_{jr}^n$.
- Set step number $k = 0$.

Iteration $k + 1$ of the fixed point procedure: Calculation of the isentropic solution guess.

- Solve $\forall j \in \mathcal{J}$,

$$\begin{cases} \bar{\tau}_j^{n,k+1} = \tau_j^n + \frac{\Delta t}{M_j} \sum_{r \in \mathcal{R}_j} \langle \mathbf{D}_{jr}^{n,k}, \bar{\mathbf{u}}_r^{n,k+1} \rangle, \\ \bar{\mathbf{u}}_j^{n,k+1} = \mathbf{u}_j^n - \frac{\Delta t}{M_j} \sum_{r \in \mathcal{R}_j} \bar{\mathbf{F}}_{jr}^{n,k+1}, \\ \bar{S}_j^{n,k+1} = S_j^n, \end{cases}$$

with

$$\begin{cases} \bar{\mathbf{F}}_{jr}^{n,k+1} = A_{jr}^n (\bar{\mathbf{u}}_j^{n,k+1} - \bar{\mathbf{u}}_r^{n,k+1}) + \mathbf{D}_{jr}^{n,k} \bar{p}_j^{n,k+1}, \\ \sum_{j \in \mathcal{J}_r} \bar{\mathbf{F}}_{jr}^{n,k+1} = \mathbf{0}. \end{cases}$$

- Compute $\forall r \in \mathcal{R}$, $\bar{\mathbf{x}}_r^{n,k+1} = \mathbf{x}_r^n + \Delta t \bar{\mathbf{u}}_r^{n,k+1}$.
- Compute $\forall j \in \mathcal{J}$, $V_j^{n,k+1} = \frac{1}{d} \sum_{r \in \mathcal{R}_j} \langle \mathbf{C}_{jr}^{n,k+1}, \bar{\mathbf{x}}_r^{n,k+1} \rangle$
- If $\max_{j \in \mathcal{J}} \left| 1 - \frac{M_j}{V_j^{n,k+1}} \bar{\tau}_j^{n,k+1} \right| > \varepsilon$ compute $\mathbf{D}_{jr}^{n,k+1}$, set $k \leftarrow k + 1$ and compute next **Iteration** $k + 1$ else compute **Correction**.

Correction: Restore total energy conservation and physical entropy growth.

- Update conservative quantities $\forall j \in \mathcal{J}$,

$$\begin{cases} \tau_j^{n+1} = \tau_j^n + \frac{\Delta t}{M_j} \sum_{r \in \mathcal{R}_j} \langle \mathbf{D}_{jr}^{n,k}, \bar{\mathbf{u}}_r^{n,k+1} \rangle, \\ \mathbf{u}_j^{n+1} = \mathbf{u}_j^n - \frac{\Delta t}{M_j} \sum_{r \in \mathcal{R}_j} \bar{\mathbf{F}}_{jr}^{n,k+1}, \\ E_j^{n+1} = E_j^n - \frac{\Delta t}{M_j} \sum_{r \in \mathcal{R}_j} \langle \bar{\mathbf{F}}_{jr}^{n,k+1}, \bar{\mathbf{u}}_r^{n,k+1} \rangle. \end{cases}$$

Mesh displacement: Move the nodes using the converged velocity

- Compute $\forall r \in \mathcal{R}$, $\mathbf{x}_r^{n+1} = \mathbf{x}_r^n + \Delta t \bar{\mathbf{u}}_r^{n,k+1}$.

Note that each loop (iteration k) of the fixed point procedure in the predictor step is an implicit non linear problem that we solve with a Newton's method without any problem. We do not know how to assess the convergence or the rate of convergence of the fixed point procedure even if our tests show that it converges pretty well. We prefer to rely on numerical experiments to evaluate the properties of this method. Thus, we encourage the reader to go to the numerical results Section 6.

5 Implicit and explicit coupled schemes

In practice, one may not want to use the implicit scheme in the whole domain. Indeed, the calculation of the solution to the nonlinear system may be expensive. Thus, it is better to use the implicit scheme in limited regions that might impose a very small time step compared with the rest of the domain. This small time step restriction is relaxed with the use of our implicit scheme. In [20] we proposed such an approach with success in dimension $d = 1$.

The implicit-explicit coupling that we have detailed in our previous work [20] is naturally extended to higher dimensions $d \geq 2$. Let us just write the prediction step in that case, the correction step is unchanged. Let us denote respectively by \mathcal{J}^{exp} the sets of cells treated explicitly and by \mathcal{J}^{imp} the sets of cells treated implicitly. One has $\mathcal{J} = \mathcal{J}^{\text{exp}} \sqcup \mathcal{J}^{\text{imp}}$. Let us also define the set of interface nodes connected to implicit and explicit cells

$$\mathcal{R}^{\text{imp}} = \{r \in \mathcal{R} / \mathcal{J}_r \cap \mathcal{J}^{\text{exp}} \neq \emptyset \text{ and } \mathcal{J}_r \cap \mathcal{J}^{\text{imp}} \neq \emptyset\}.$$

The cells treated implicitly have to satisfy the equations

$$\forall j \in \mathcal{J}^{\text{imp}}, \begin{cases} \bar{\tau}_j = \tau_j^n + \frac{\Delta t}{M_j} \sum_{r \in \mathcal{R}_j} \langle \mathbf{D}_{jr}, \bar{\mathbf{u}}_r \rangle, \\ \bar{\mathbf{u}}_j = \mathbf{u}_j^n - \frac{\Delta t}{M_j} \sum_{r \in \mathcal{R}_j} \bar{\mathbf{F}}_{jr}, \\ \bar{S}_j = S_j^n, \end{cases}$$

where

$$\forall j \in \mathcal{J}_r \cap \mathcal{J}^{\text{imp}}, \forall r \in \mathcal{R}_j, \quad \bar{\mathbf{F}}_{jr} = A_{jr}(\bar{\mathbf{u}}_j - \bar{\mathbf{u}}_r) + \mathbf{D}_{jr} \bar{p}_j.$$

The cells treated explicitly have to satisfy the equations

$$\forall j \in \mathcal{J}^{exp}, \quad \begin{cases} \tau_j^{n+1} = \tau_j^n + \frac{\Delta t}{M_j} \sum_{r \in \mathcal{R}_j} \langle \mathbf{C}_{jr}^n, \mathbf{u}_r^n \rangle, \\ \mathbf{u}_j^{n+1} = \mathbf{u}_j^n - \frac{\Delta t}{M_j} \sum_{r \in \mathcal{R}_j} \mathbf{F}_{jr}^n, \end{cases}$$

where

$$\forall j \in \mathcal{J}_r \cap \mathcal{J}^{exp}, \forall r \in \mathcal{R}_j, \quad \mathbf{F}_{jr}^n = A_{jr}(\mathbf{u}_j^n - \bar{\mathbf{u}}_r) + \mathbf{C}_{jr}^n p_j^n.$$

The equality of forces at all nodes is enforced

$$\forall r \in \mathcal{R}, \quad \sum_{j \in \mathcal{J}_r \cap \mathcal{J}^{imp}} \bar{\mathbf{F}}_{jr} + \sum_{j \in \mathcal{J}_r \cap \mathcal{J}^{exp}} \mathbf{F}_{jr}^n = \mathbf{0}.$$

This equation couples cells in the implicit region with cells in the explicit region.

Then the linear system for the calculation of the velocities and pressures is carefully assembled, retaining only the linear equations that must be treated implicitly. We solve the implicit problem which provides the implicit node velocities that are used to solve the explicit part. Then, the cell volumes are updated using the new node coordinates in both regions. So, the scheme is also conservative in volume. It is easy to check that after the correction step, the overall scheme is conservative in mass, momentum and total energy.

6 Numerical results

In this Section, we provide numerical examples calculated with the Algorithm of this work, and we use the standard library PETCs for solving the linear systems. These test cases assess the correct behavior of the implicit scheme proposed in this paper in dimension 2 and 3. We present two kinds of tests. The first ones illustrate the robustness of the approach. The second ones are more practical examples which enlighten the kind of applications that could benefit from using this scheme.

Since we have no theoretical analysis for the convergence of neither the Newton method nor the geometrical fixed point algorithm given in Section 4, we find it educative to use quite demanding convergence criteria. Thus, we use the following tuning for all the following tests. The convergence criterion for the Newton method is set to 10^{-12} and the criterion for the geometry is set to 10^{-4} .

6.1 Sod shock tube

For this first test, we solve the classical Sod shock tube in 2D and 3D using unstructured grid. The setting is the following. Initial data is

$$\rho(\mathbf{x}, t = 0) = \begin{cases} 1 & \text{if } x < 0.5, \\ 0.125 & \text{else,} \end{cases} \quad \mathbf{u}(\mathbf{x}, t = 0) = \mathbf{0}, \quad p(\mathbf{x}, t = 0) = \begin{cases} 1 & \text{if } x < 0.5, \\ 0.1 & \text{else.} \end{cases}$$

The pressure follows a perfect gas law with $\gamma = 1.4$. The computation is run until time $t = 0.2$. Sliding (or symmetry) boundary conditions are imposed on the boundaries of the domain³.

The results are discussed in two separate parts. First we illustrate the robustness of the proposed method and second we show the evolution of precision with regard to the explicit scheme while increasing CFL.

6.1.1 Robustness

To illustrate the robustness of the method, we run the test using only one time step: $\Delta t = t_{\max} = 0.2$ on unstructured grids in both 2D and 3D. In 2D, the mesh contains both triangles and quadrilaterals. In 3D, it is composed of tetrahedra, pyramids, prisms and hexahedra.

³Actually, it is important to fix the corners of domain, and in 3D to treat the sliding on the edges of the domain. If not, the convergence of the full algorithm can be much more difficult.

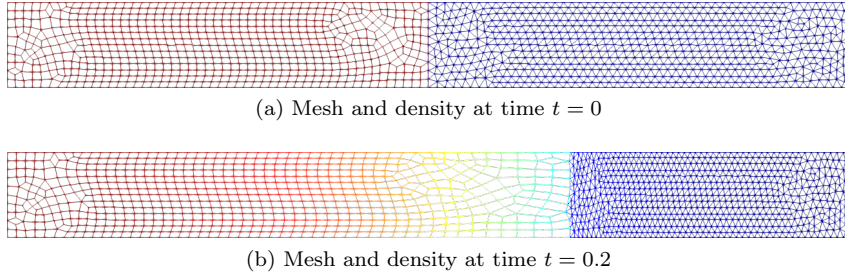


Figure 2: Sod test using a 2D unstructured grid. Result is obtained using a single time step: $\Delta t = 0.2$.

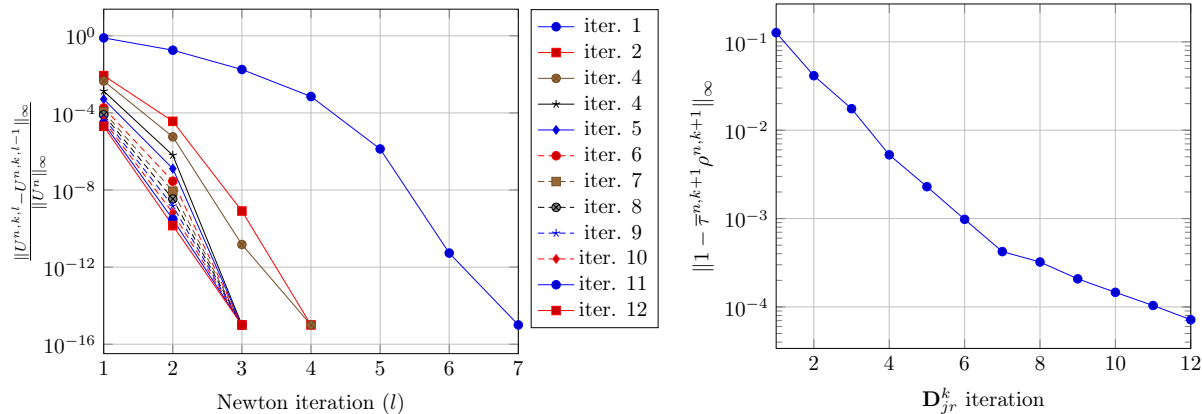


Figure 3: Sod calculation in 2D. $\Delta t = 0.2$. **Left:** Newton convergence (l) for each fixed point iteration (k). **Right:** Fixed point convergence (k).

In Figures 2 and 4, we represent the meshes colored by density in 2D and 3D. The obtained solutions for such large time step are reasonable and we discuss them more precisely in the next Section.

Figures 3 and 5 display the convergence history of the whole method in both 2D and 3D. On the right, we plot the convergence of the error in density

$$k \mapsto \left\| 1 - \bar{\tau}^{n,k+1} \rho^{n,k+1} \right\|$$

which allows the evaluation of the convergence of the fixed point method in each case. One observes a monotone convergence to a fixed point. The maximum volume error is reduced to a maximum of 10^{-4} by around ten iterations.

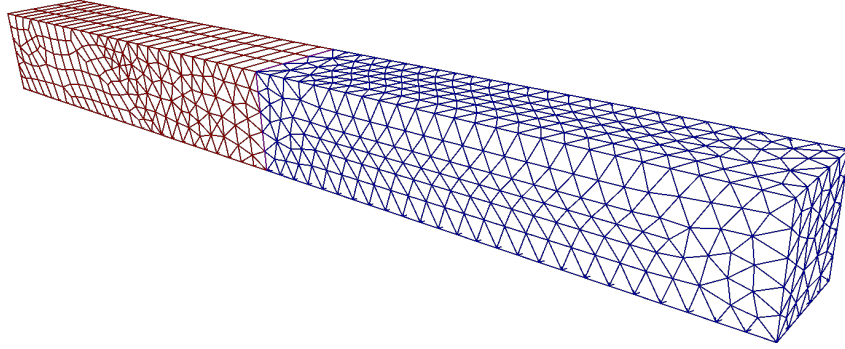
On the left, we plot for each fixed point iteration the convergence history of the Newton method that is used to solve the isentropic predictor. Again in this case, one observes a monotone convergence. A maximum number of 7 iterations is required to solve the non linear problem at machine precision. One also observes that the first fixed point step is the one that requires the more iterations.

6.1.2 Precision

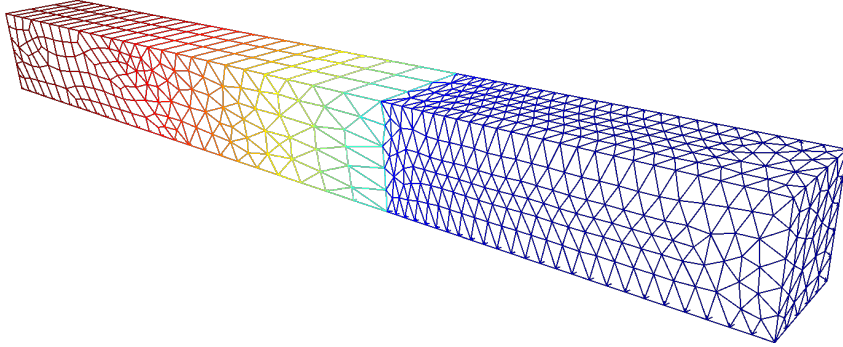
We now discuss the precision of the method with regard to the CFL number. Here we only present the 2D case since 3D results are similar. In Figures 6a, 6b and 6c we compare the numerical solution obtained for the explicit scheme (using a CFL number of 0.4) to the solutions of the implicit scheme using CFL numbers of 0.4, 1 and 5.

Using the explicit CFL number 0.4, one observes that the solution of implicit and explicit schemes are quite close (see Figures 6a). As expected, the numerical dissipation increases with CFL number (see Figures 6b and 6c). However, as we have already observed and explained in 1D [20] in the case of 1D Riemann problems the contact discontinuity position is very accurate even for very large CFL numbers.

Finally in Figure 6 we compare a cut of the density field of the 2D calculation with the 1D result when using the maximum time step $\Delta t = 0.2$. Solutions are almost superposed. Obviously for such a large time step, the solution is excessively dissipated, but the contact discontinuity location remains



(a) Mesh and density at time $t = 0$



(b) Mesh and density at time $t = 0.2$

Figure 4: Sod test using a 3D unstructured grid. Result is obtained using a single time step: $\Delta t = 0.2$.

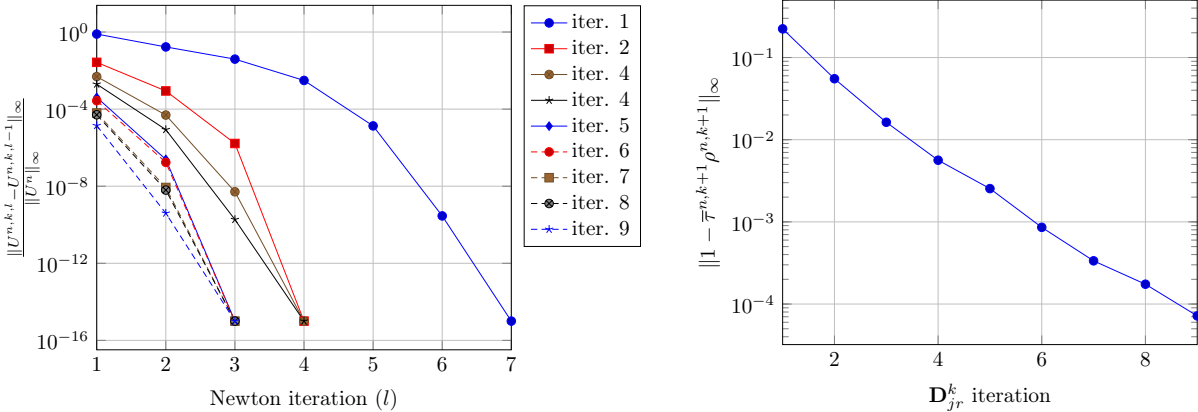


Figure 5: Sod calculation in 3D. $\Delta t = 0.2$. **Left:** Newton convergence (l) for each fixed point iteration (k). **Right:** Fixed point convergence (k).

quite good. Moreover, as we explained it in [20] the left shift is due to the interaction with boundary conditions. Using a larger domain, the contact discontinuity is almost perfectly placed (see [20] for details and an analysis of this behavior).

6.2 Saltzman test case

This test is a classical test of robustness for Lagrangian schemes. Actually the difficulty is twofold, since the pressure is initially almost null and this piston problem is solved on a perturbed grid which is not aligned with the shock. The pressure being almost null, this problem is singular at the limit of vanishing pressure. In this regime the Saltzman problem is not covered by Theorem 1 because the J becomes singular, so we expect non convergence of our algorithms for large time steps.

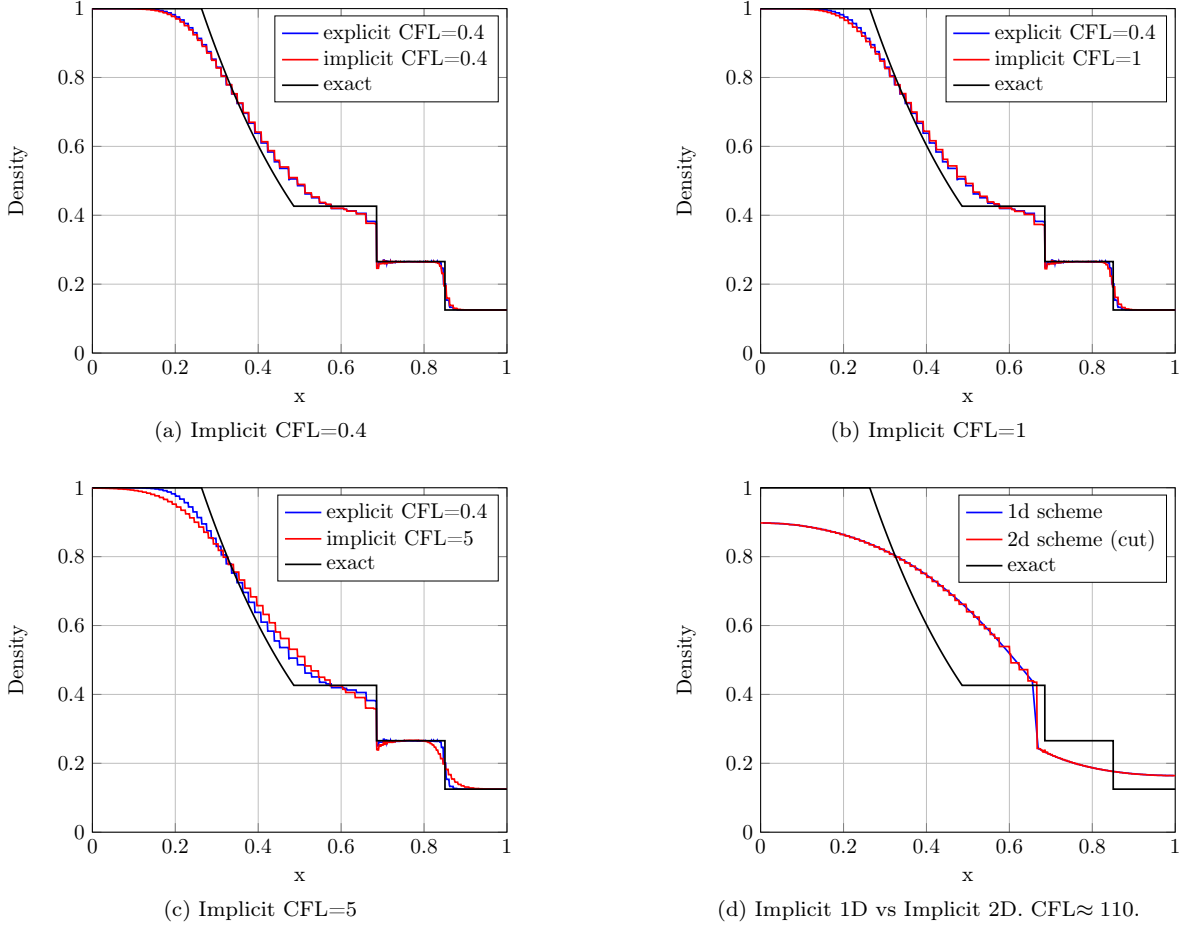


Figure 6: Density plot at time $t = 0.2$. Illustration of the quality of the approximation of the implicit scheme with regard to the CFL number.

The computational domain is $\Omega =]0, 1[\times]0, 0.1[$ which is meshed using a uniform 100×10 grid that is perturbed by displacing its nodes as

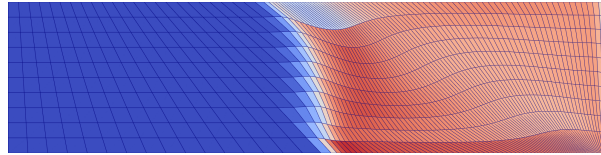
$$\begin{cases} \tilde{x} = x + 0.1(1 - 20y) \sin(\pi x), \\ \tilde{y} = y. \end{cases}$$

Initial data is set as

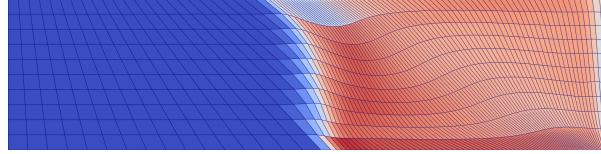
$$(\rho, \mathbf{u}, p) = (1, \mathbf{0}, 10^{-4}),$$

where the pressure p follows a perfect gas law with $\gamma = \frac{5}{3}$. On each boundary we impose wall conditions except on the right boundary where a constant normal velocity of -1 is prescribed.

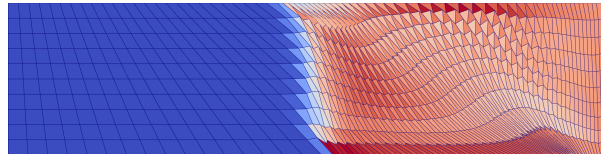
In Figure 7 we compare the obtained meshes at time $t = 0.6$ using the explicit scheme and with the implicit scheme for two time stepping strategies. One first observes that numerical solutions are remarkably close for this difficult test. The agreement for the shock location is notable. The explicit solution (see Figure 7a) is obtained using $\text{CFL} = 0.02$, which is approximately the maximum value that we can take to run the calculation. Figure 7b depicts the solution for the implicit solver using $\text{CFL} = 0.05$. One notices the similarities with regard to the mesh deformation for a 2.5 times larger CFL. Finally, in Figure 7c we show the result obtained with the implicit scheme using a constant time step $dt = 10^{-2}$ (which corresponds more or less to $\text{CFL} = 10$). One observes that if the solution remains close to the explicit one, the mesh displays oscillations. Since this is almost the maximum time step that allows the fixed point method to converge, an interpretation is that these oscillations illustrate the stability limit experienced for this test.



(a) Explicit scheme CFL = 0.02



(b) Implicit scheme CFL = 0.05



(c) Implicit scheme $\Delta t = 0.01$ (CFL ≈ 10)

Figure 7: Comparison of explicit scheme and different CFL numbers for the implicit scheme at time $t = 0.6$. Density color map is fixed between 1 and 5 to ease comparison.

In our view these results assess the robustness of the method. Even if the method fails for arbitrary time step, it allows the use of much larger time steps than the explicit version. The gain of time step is in this case

$$\frac{\Delta t_{\text{imp}}}{\Delta t_{\text{exp}}} = 500.$$

6.3 Converging Sod shock tube with a rebound

This test is an example of a potential application of the method. It is quite common for ICF (Inertial Confinement Fusion) simulation to study the growth of interface perturbations. To do so, a classical strategy consists in using polar grids (see Figure 8) that allow to capture symmetries of radial flows. The main drawback of this strategy is that cells at the center of the flow are very small and may constrain the time step, increasing the whole computational cost.

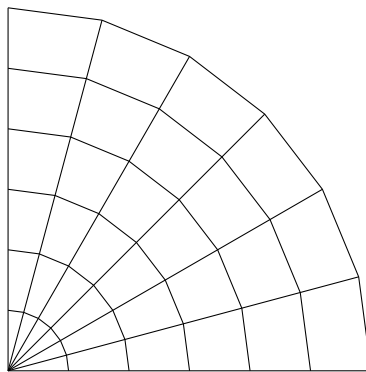


Figure 8: Example of a polar grid of Ω .

The test problem below models this behavior, but without the perturbations to focus on the stability of the method. It consists in a convergent Sod shock tube. The computational domain is

$$\Omega = \{ \mathbf{x} \in \mathbb{R}^2 \text{ s.t. } x_1 > 0, x_2 > 0 \text{ and } \|\mathbf{x}\| < 1 \}.$$

The initial data is

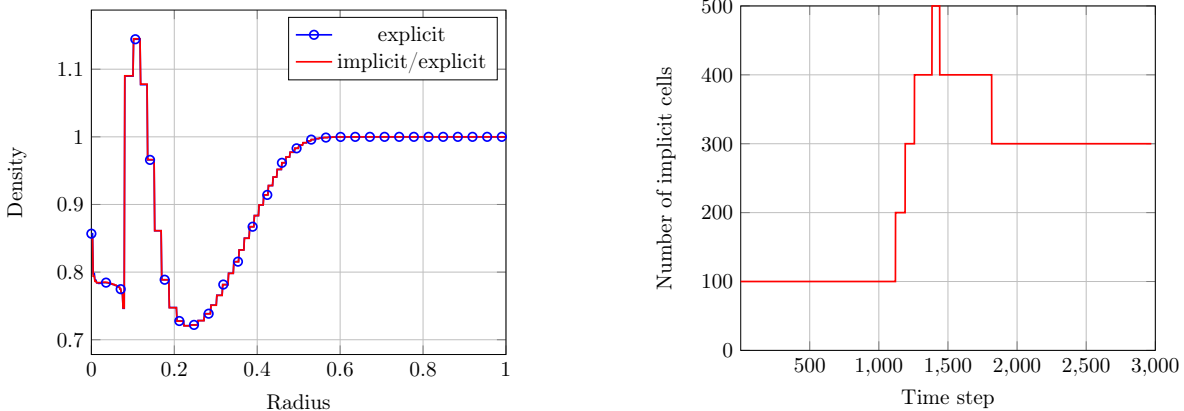
$$\rho(\mathbf{x}, t = 0) = \begin{cases} 1 & \text{if } \|\mathbf{x}\| > 0.3, \\ 0.125 & \text{else,} \end{cases} \quad \mathbf{u}(\mathbf{x}, t = 0) = \mathbf{0}, \quad p(\mathbf{x}, t = 0) = \begin{cases} 1 & \text{if } \|\mathbf{x}\| > 0.3, \\ 0.1 & \text{else.} \end{cases}$$

The pressure follows a perfect gas law and we set $\gamma = 1.4$. Notice that the initial discontinuity is set at radius 0.3 so that the shock bounces back on $\mathbf{x} = \mathbf{0}$ approximately at time $t = 0.1$. Final time is set to $t = 0.2$. A 100×100 polar mesh of Ω (100 layers and 100 sectors) is used to perform calculations.

Here we try a different strategy with the implicit/explicit scheme explained in Section 5. The cells that are treated with the implicit scheme are the ones that require a time step smaller than 5×10^{-5} , so the implicit region evolves through time. Thus time step is defined only by the cells that are treated explicitly.

Results are presented in Figure 9. The solutions obtained using the reference explicit scheme and the implicit/explicit strategy are almost superposed (see Figure 9a). One should notice that the number of time steps used to compute the solution decreases from 17751 in the explicit case to 2969 when using implicit cells where the required local time step is below 5×10^{-5} , a ratio of approximately 6. The total computational cost using the implicit/explicit approach is pretty much reduced by a factor $\frac{1}{3}$. In Figure 9b we plot the number of implicit cells for each time step. Since the radial symmetry is perfectly preserved by the scheme, one observes that the number of implicit cells evolves by sets of 100 cells. It corresponds to the number of cells in each layer of the polar grid.

For this problem, one observes that the implicit/explicit scheme relaxes the time step constraint at the center of the domain of calculation, still with the same numerical solution.



(a) Comparison of the explicit solution with the implicit/explicit. Density, radial cut at time $t = 0.2$.

(b) Number of implicit cells according to the iteration.

Figure 9: Implicit/explicit scheme for the converging Sod shock tube.

7 Conclusion

In this paper we proposed and analyzed an extension of our previous work [20] to dimensions 2 and 3. The proposed method is an implicit finite volume discretization for compressible Euler in semi-Lagrangian coordinates. It can be decomposed as a three-step algorithm that treats separately the different kinds of non-linearities. The first step consists in solving isentropic Euler equations. It handles the non-linearity due to the equation of state (at fixed entropy). This non-linear step is solved using Newton's method. This problem is well-posed in the sense that it admits a unique solution that lives in the invariant domain. This solution is entropy stable which is a strong guarantee of numerical stability. The second step is the restoration of the total energy conservation and treats the non-linearity due to the work of the pressure forces ($\nabla \cdot p\mathbf{u}$). Actually, this step is free since it is explicit: pressure and velocity fluxes are the ones computed in the first step. This step ensures physical entropy growth. The third step is the mesh motion $\mathbf{x}_r^{n+1} = \mathbf{x}_r^n + \Delta t \bar{\mathbf{u}}_r$. Starting from dimension 2, the cell volume computed according

to these new node positions may differ with regard to the one resulting of the continuity equation, so that $\rho_j^{n+1} = \frac{M_j}{V_j^{n+1}} \neq \frac{1}{\tau_j}$, which can break the stability of the method when chaining time steps. This is the result of potential non-linearities of the deformation of the cells. This last non-linearity is treated using a fixed-point method that ensures $\bar{V}_j = V_j^{n+1}$ at convergence. This restores the entropy stability of the whole procedure. We have also explained how to couple the implicit and explicit schemes, which is probably more suited for applications. From the numerical point of view, we proposed numerical experiments that illustrate the behavior of the method.

With regard to the numerical analysis of the scheme a few questions remain to be addressed. Firstly, we always observe a very good behavior of Newton's method. This is something that we do not explain yet. The structure of the third derivative of the functional $J(U)$ is quite simple, the analysis of this Newton's method might be possible. Secondly, as expected and experimented on Saltzman test which is a singular test problem at the limit of the theory, the fixed point method used to treat the geometrical non-linearity becomes marginally stable. It seems quite difficult to analyze, but obviously a convergence analysis in the regime of vanishing pressure would be of practical interest.

A Entropy stability of the prediction step

The aim of this Section is to prove Proposition 3: the predictor-scheme (30)–(31) satisfies the entropy inequality (46), that is $M_j \frac{\bar{E}_j - E_j^n}{\Delta t} + \sum_{r \in \mathcal{R}_j} \langle \bar{\mathbf{F}}_{jr}, \bar{\mathbf{u}}_r \rangle \leq 0$.

Rewrite E as a function of $U := (\tau, \mathbf{u}, S)$. According to the Gibbs formula

$$dE = -pd\tau + \langle \mathbf{u}, d\mathbf{u} \rangle + TdS,$$

thus

$$\nabla_U E = \begin{pmatrix} -p \\ \mathbf{u} \\ T \end{pmatrix}.$$

Since E is a convex function of U , for two arbitrary states $U_i = (\tau_i, \mathbf{u}_i, S_i)$, $i \in \{1, 2\}$, one has

$$E(U_1) - E(U_2) \leq \langle \nabla_U E|_{U_1}, (U_1 - U_2) \rangle.$$

Let us now choose $U_1 = \bar{U}_j$ and $U_2 = U_j^n$. Here $j \in \mathcal{J}$ designates a cell, U_j^n is the state in this cell at time t^n and \bar{U}_j is the result of the predictor scheme (30)–(31).

So, we have

$$\forall j \in \mathcal{J}, \quad E(\bar{U}_j) - E(U_j^n) \leq \langle \nabla_U E|_{\bar{U}_j}, (\bar{U}_j - U_j^n) \rangle,$$

which rewrites using the scheme notations

$$\forall j \in \mathcal{J}, \quad \bar{E}_j - E_j^n \leq \left\langle \begin{pmatrix} -\bar{p}_j \\ \bar{\mathbf{u}}_j \\ \bar{T}_j \end{pmatrix}, \begin{pmatrix} \bar{\tau}_j - \tau_j^n \\ \bar{\mathbf{u}}_j - \mathbf{u}_j^n \\ \bar{S}_j - S_j^n \end{pmatrix} \right\rangle.$$

One now substitutes the scheme (30)–(31), remembering that $\bar{S}_j = S_j^n$ during the isentropic step, and gets

$$\forall j \in \mathcal{J}, \quad \bar{E}_j - E_j^n \leq \left\langle \begin{pmatrix} -\bar{p}_j \\ \bar{\mathbf{u}}_j \\ \bar{T}_j \end{pmatrix}, \begin{pmatrix} \frac{\Delta t}{M_j} \sum_{r \in \mathcal{R}_j} \langle \mathbf{D}_{jr}, \bar{\mathbf{u}}_r \rangle \\ -\frac{\Delta t}{M_j} \sum_{r \in \mathcal{R}_j} \bar{\mathbf{F}}_{jr} \\ 0 \end{pmatrix} \right\rangle,$$

which rewrites

$$\forall j \in \mathcal{J}, \quad \frac{M_j}{\Delta t} (\bar{E}_j - E_j^n) \leq -\bar{p}_j \sum_{r \in \mathcal{R}_j} \langle \mathbf{D}_{jr}, \bar{\mathbf{u}}_r \rangle - \left\langle \bar{\mathbf{u}}_j, \sum_{r \in \mathcal{R}_j} \bar{\mathbf{F}}_{jr} \right\rangle.$$

Injecting on both sides $\sum_{r \in \mathcal{R}_j} \langle \bar{\mathbf{F}}_{jr}, \bar{\mathbf{u}}_r \rangle$, it rewrites after few manipulations

$$\forall j \in \mathcal{J}, \quad \frac{M_j}{\Delta t} (\bar{E}_j - E_j^n) + \sum_{r \in \mathcal{R}_j} \langle \bar{\mathbf{F}}_{jr}, \bar{\mathbf{u}}_r \rangle \leq -\bar{p}_j \sum_{r \in \mathcal{R}_j} \langle \mathbf{D}_{jr}, \bar{\mathbf{u}}_r \rangle + \sum_{r \in \mathcal{R}_j} \langle \bar{\mathbf{F}}_{jr}, \bar{\mathbf{u}}_r - \bar{\mathbf{u}}_j \rangle.$$

Finally, we replace $\overline{\mathbf{F}}_{jr}$ by its definition (31) which gives

$$\forall j \in \mathcal{J}, \quad \frac{M_j}{\Delta t} (\overline{E}_j - E_j^n) + \sum_{r \in \mathcal{R}_j} \langle \overline{\mathbf{F}}_{jr}, \overline{\mathbf{u}}_r \rangle \leq -\overline{p}_j \sum_{r \in \mathcal{R}_j} \langle \mathbf{D}_{jr}, \overline{\mathbf{u}}_r \rangle + \sum_{r \in \mathcal{R}_j} \langle A_{jr}(\overline{\mathbf{u}}_j - \overline{\mathbf{u}}_r) + \mathbf{D}_{jr} \overline{p}_j, \overline{\mathbf{u}}_r - \overline{\mathbf{u}}_j \rangle,$$

which is rearranged as

$$\forall j \in \mathcal{J}, \quad \frac{M_j}{\Delta t} (\overline{E}_j - E_j^n) + \sum_{r \in \mathcal{R}_j} \langle \overline{\mathbf{F}}_{jr}, \overline{\mathbf{u}}_r \rangle \leq - \sum_{r \in \mathcal{R}_j} (\overline{\mathbf{u}}_j - \overline{\mathbf{u}}_r)^T A_{jr} (\overline{\mathbf{u}}_j - \overline{\mathbf{u}}_r) - \sum_{r \in \mathcal{R}_j} \langle \mathbf{D}_{jr} \overline{p}_j, \overline{\mathbf{u}}_r - \overline{\mathbf{u}}_j \rangle.$$

Since A_{jr} matrices are non-negative, it ends the proof.

References

- [1] E. Abbate, A. Iollo, and G. Puppo. An all-speed relaxation scheme for gases and compressible materials. *Journal of Computational Physics*, 351:1–24, 2017.
- [2] Satish Balay, William Gropp, Lois Curfman McInnes, and Barry F Smith. Petsc, the portable, extensible toolkit for scientific computation. *Argonne National Laboratory*, 2(17), 1998.
- [3] R. M. Beam and R. F. Warming. An Implicit Finite-Difference Algorithm for Hyperbolic Systems in Conservation-Law Form. *Journal of Computational Physics*, 22(1):87–110, 1976.
- [4] F. Bouchut, C. Chalons, and S. Guisset. An entropy satisfying two-speed relaxation system for the barotropic Euler equations: application to the numerical approximation of low Mach number flows. *Numerische Mathematik*, 145:35–76, 2020.
- [5] L. Brugnano and V. Casulli. Iterative Solution of Piecewise Linear Systems. *SIAM J. Sci. Comput.*, 30:463–472, 2008.
- [6] G. Carré, S. Del Pino, B. Després, and E. Labourasse. A cell-centered lagrangian hydrodynamics scheme on general unstructured meshes in arbitrary dimension. *J. Comp. Phys.*, 228, 5160–5183, 2009.
- [7] C. Chalons, F. Coquel, and C. Marmignon. Time-Implicit Approximation of the Multipressure Gas Dynamics Equations in Several Space Dimensions. *SIAM*, 48:1678–1706, 2010.
- [8] S. Del Pino, B. Després, and A. Plessier. Moving grids and cell volume calculations. *HAL CEA*, March 2024. URL: <https://cea.hal.science/cea-04489104>.
- [9] B. Després. Weak Consistency of the Cell-Centered Lagrangian GLACE Scheme on General Meshes in Any Dimension. *Computer Methods in Applied Mechanics and Engineering*, 199(41):2669–2679, 2010.
- [10] B. Després and C. Mazeran. Lagrangian Gas Dynamics in Two Dimensions and Lagrangian systems. *Arch. Rational Mech. Anal*, 2005.
- [11] B. Després. *Numerical Methods for Eulerian and Lagrangian Conservation Laws*. Birkhäuser Basel, 2017.
- [12] B. A. Fryxell, P. R. Woodward, P. Colella, and K.-H. Winkler. An Implicit-Explicit Hybrid Method for Lagrangian Hydrodynamics. *Journal of Computational Physics*, 63:283–310, 1986.
- [13] T. Gallouët, L. Gastaldo, R. Herbin, and J.-C. Latché. An Unconditionally Stable Pressure Correction Scheme for the Compressible Barotropic Navier-Stokes Equations. *ESAIM: M2AN*, 42:303–331, 2008.
- [14] G. Georges, J. Breil, and P.-H. Maire. A 3d gcl compatible cell-centered lagrangian scheme for solving gas dynamics equations. *J. Comp. Phys.*, 305 921–941, 2016.

- [15] R. I. Issa. Solution of the Implicitly Discretised Fluid Flow Equations by Operator-Splitting. *Journal of Computational Physics*, 62:40–65, 1985.
- [16] E. Labourasse and B. Després. Stabilization of cell-centered compressible lagrangian method using subzonal entropy. *Journal of Computational Physics*, 231, 2012.
- [17] P-H. Maire, R. Abgrall, J. Breil, and J. Ovardia. A cell-centered Lagrangian scheme for two dimensional compressible flow problems. *SIAM J. Sci. Comput.*, 29(4):1781-1824, 2007.
- [18] C. Mazeran. *Thèse: Sur la Structure Mathématique et l'Approximation Numérique de l'Hydrodynamique Lagrangienne Bidimensionnelle*. Université de Bordeaux I, 2007.
- [19] A. Plessier. *Implicit semi-Lagrangian schemes for compressible gas dynamics*. Theses, Sorbonne Université, May 2023. URL: <https://theses.hal.science/tel-04135003>.
- [20] A. Plessier, S. Del Pino, and B. Després. Implicit discretization of Lagrangian gas dynamics. *ESAIM: M2AN*, 57(2):717–743, 2023.
- [21] G. Puppo, M. Semplice, and G. Visconti. Quinpi: integrating conservation laws with CWENO implicit methods. *Communications on Applied Mathematics and Computation*, 5(1):343–369, 2023.
- [22] P.-A. Raviart and E. Godlewski. *Numerical Approximation of Hyperbolic Systems of Conservation Laws*. Springer, 1996.
- [23] A. Thomann, A. Iollo, and G. Puppo. Implicit Relaxed All Mach Number Schemes for Gases and Compressible Materials. *SIAM Journal on Scientific Computing*, 45(5):A2632–A2656, 2023.
- [24] A. Thomann, M. Zenk, G. Puppo, and Klingenberg. An all-speed second order IMEX relaxation scheme for the Euler equations. *Communications in Computational Physics*, 28:591–620, 2020.
- [25] E. F. Toro. *Riemann Solvers and Numerical Methods for Fluid Dynamics*. Springer Verlag, 1999.
- [26] G. Toth, R. Keppens, and M. A. Bochev. Implicit and Semi-Implicit Schemes in the Versatile Advection Code: Numerical Tests. *Astronomy and Astrophysics*, 332:1159 – 1170, 1998.
- [27] R. Tyrrell Rockafellar. *Convex Analysis*. Princeton University Press, 1970.
- [28] D. R. Van der Heuk, C. Vuik, and P. Wesseling. A Conservative Pressure-Correction Method for Flow at All Speed. *Computers and Fluids*, 32:1113 – 1132, 2003.